J Biomol NMR (2012) 54:135–143
DOI 10.1007/s10858-012-9667-9

COMMUNICATION

3D-TROSY-based backbone and ILV-methyl resonance assignments of a 319-residue homodimer from a single protein sample

Anna Krejcirikova · Vitali Tugarinov

Received: 12 July 2012 / Accepted: 29 August 2012 / Published online: 8 September 2012

Abstract The feasibility of practically complete backbone and ILV methyl chemical shift assignments from a single [U-^{2}H,^{15}N,^{13}C; Ileδ1-{$^{13}CH_3$}; Leu,Val-{$^{13}CH_3$/$^{12}CD_3$}]-labeled protein sample of the truncated form of ligand-free *Bst*-Tyrosyl tRNA Synthetase (*Bst*-ΔYRS), a 319-residue predominantly helical homodimer, is established. Protonation of ILV residues at methyl positions does not appreciably detract from the quality of TROSY triple resonance data. The assignments are performed at 40 °C to improve the sensitivity of the measurements and alleviate the overlap of ^{1}H–^{15}N correlations in the abundant α-helical segments of the protein. A number of auxiliary approaches are used to assist in the assignment process: (1) selection of ^{1}H–^{15}N amide correlations of certain residue types (Ala, Thr/Ser) that simplifies 2D ^{1}H–^{15}N TROSY spectra, (2) straightforward identification of ILV residue types from the methyl-detected 'out-and-back' HMCM(CG)CBCA experiment, and (3) strong sequential HN–HN NOE connectivities in the helical regions. The two subunits of *Bst*-YRS were predicted earlier to exist in two different conformations in the absence of ligands. In agreement with our earlier findings (Godoy-Ruiz in J Am Chem Soc 133:19578–195781, 2011), no evidence of dimer asymmetry has been observed in either amide- or methyl-detected experiments.

Keywords Chemical shifts assignments · Deuteration · TROSY · In vitro re-folding · Methyl labeling

Introduction

The enzyme Tyrosyl tRNA Synthetase (YRS) (Fersht 1987, 2002) catalyzes the activation of Tyr via formation of Tyr-AMP and subsequent transfer of the activated Tyr to the cognate tRNA^{Tyr}. YRS from the thermophilic organism *Bacillus stearothermophilus* (*Bst*-YRS; full-length YRS MW = 95 kDa) is a paradigmatic example of a 'half-site-reactive' homodimer (Fersht 2002; Ward and Fersht 1988a, b). YRS exhibits 'half-of-the-sites' activity (extreme form of negative cooperativity) with respect to Tyr binding, Tyr-AMP formation and tRNA charging: it binds to, activates, and charges tRNA with only 1 mol of Tyr per mole of dimer (Fersht 1975; Ward and Fersht 1988b). YRS was predicted to be asymmetrical in solution in the absence of ligands from extensive kinetic and mutagenesis studies (Fersht 2002; Ward and Fersht 1988b). The truncated form of the enzyme lacking the C-terminal tRNA-binding domain (ΔYRS; MW = 72 kDa) can activate Tyr with the same efficiency as the full-length enzyme but cannot charge tRNA (Waye et al. 1983). The ΔYRS dimer retains the 'half-site-activity' with respect to Tyr binding and activation.

Several crystal structures of *Bst*-YRS have been solved: free, in complexes with Tyr-AMP and inhibitors (Brick et al. 1989). The structure of the C-terminal domain of YRS that is not observed in any of the available crystal structures, has been solved separately by NMR (Guijarro

Electronic supplementary material The online version of this article (doi:10.1007/s10858-012-9667-9) contains supplementary material, which is available to authorized users.

A. Krejcirikova · V. Tugarinov (✉)
Department of Chemistry and Biochemistry, University of Maryland, Biomolecular Sci. Bldg./CBSO, College Park, MD 20742, USA
e-mail: vitali@umd.edu

et al. 2002). All X-ray structures including that of ligand-free YRS feature a homodimer with two-fold symmetry (Brick et al. 1989; Brick and Blow 1987). The YRS dimer is one of the most compelling cases of 'pre-existent' functional asymmetry in a homodimeric protein despite that all available crystal structures are symmetric (Brick et al. 1989; Brick and Blow 1987). Although very slight differences between the conformations of the two subunits have been observed in the X-ray structure of Tyr-bound *Bst*-ΔYRS, it cannot be related to 'half-site' activity as both subunits in the crystal structure have Tyr molecules bound (Brick and Blow 1987).

Here, we establish the feasibility of complete backbone and ILV methyl chemical shift assignments in ligand-free *Bst*-ΔYRS (319-residue homodimer; MW = 72 kDa; 76 % helical content) at 40 °C (isotropic rotational correlation time $\tau_C \sim 35$ ns) using a single [U-^{2}H,^{15}N,^{13}C; Ileδ1-{^{13}CH$_3$}; Leu,Val-{^{13}CH$_3$/^{12}CD$_3$}]-labeled protein sample. The abundance of helical segments in *Bst*-ΔYRS leads to sometimes severe overlap of ^{1}H–^{15}N amide and $^{13}C^{\alpha}/^{13}C^{\beta}$ correlations in TROSY spectra, presenting significant challenges for establishing unambiguous connectivities between spin-systems. However, the protonation of ILV methyl positions does not detract significantly from the quality of TROSY triple resonance data. The assignments are facilitated by several auxiliary approaches: (1) selection of ^{1}H–^{15}N amide correlations of certain residue types (Ala, Thr/Ser) that simplifies 2D ^{1}H–^{15}N TROSY-HSQC correlation maps (Tugarinov et al. 2002), (2) straightforward identification of ILV residue types from methyl-detected 'out-and-back' experiment(s) (Tugarinov and Kay 2003), and (3) the use of strong sequential HN-HN NOE connectivities in the α-helical regions of the protein. Although 4D TROSY spectroscopy was necessary for complete backbone assignments in the 723-residue monomeric Malate Synthase G (MSG; MW = 82 kDa) (Tugarinov et al. 2002), we show that the resonances of backbone nuclei and ILV methyls of (symmetric) homodimers of a similar molecular weight can be assigned from a set of six 3D TROSY-based experiments.

The biological assembly of ΔYRS, a homodimer with nearly identical crystal structures of the two subunits (310 potentially observable amide correlations assuming symmetry) is shown in Fig. 1a (Brick and Blow 1987). Figure 1b shows the 2D ^{1}H–^{15}N TROSY correlation map of [U-^{2}H,^{15}N,^{13}C; Ileδ1-{^{13}CH$_3$}; Leu,Val-{^{13}CH$_3$/^{12}CD$_3$}]-

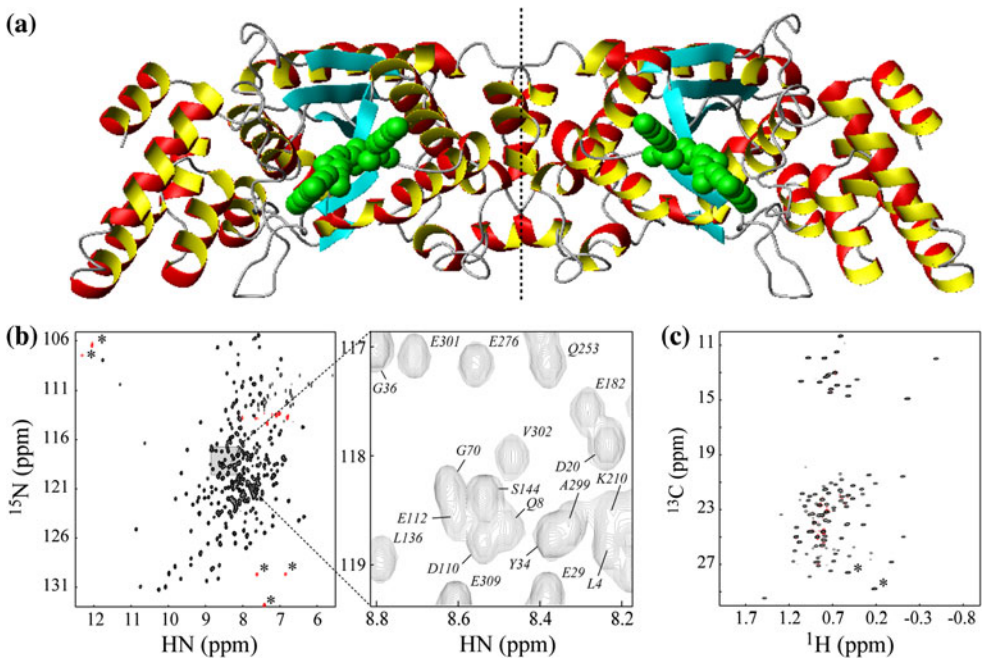

Fig. 1 **a** Ribbon representation of the structure of the biological assembly of the truncated form of *Bst*-Tyrosyl-tRNA Synthetase lacking the C-terminal tRNA-binding domain (*Bst*-ΔYRS; pdb code 1tyd (Brick and Blow 1987)). The C_2 symmetry axis of the homodimer is shown with a *dashed vertical line*. Both subunits of the molecule are shown with Tyr-AMP bound (shown with *green spheres*) although ligand-free ΔYRS has been assigned in this work. **b** 2D ^{1}H–^{15}N TROSY correlation map of the 0.8 mM (monomer concentration) ^{2}H–^{1}H back-exchanged [U-^{2}H,^{15}N,^{13}C; Ileδ1-{^{13}CH$_3$}; Leu,Val-{^{13}CH$_3$/^{12}CD$_3$}]-labeled *Bst*-ΔYRS (90 % H_2O/10 % D_2O, 600 MHz, 40 °C). The *highlighted region* of the spectrum is zoomed on the *right*, with selected assignments indicated with residue numbers. **c** Methyl ^{1}H–^{13}C CT-HMQC correlation map of the same sample as above featuring the correlations of Ile$^{\delta 1}$ and Val$^{\gamma}$/Leu$^{\delta}$ methyls. Negative peaks are shown with *red contours*. Peaks aliased in the indirect (^{15}N/^{13}C) dimensions are labeled with *asterisks*. The protein has been dissolved in the sodium phosphate buffer pH = 6.8 (no other salts added), and contained 5 mM DTT and a set of protease inhibitors (Roche)

labeled *Bst*-ΔYRS (600 MHz, 40 °C). The protein has been refolded in vitro using a fast dilution procedure very similar to that reported for MSG previously (Tugarinov, et al. 2002), in order to exchange amide deuterons in the molecular core back to protons after D_2O-based protein production (average protein recovery after in vitro refolding of ~80 %). The intensities of 28 well-resolved ^{1}H–^{15}N correlations could be recovered due to in vitro refolding of ΔYRS. Figure 1c shows methyl constant-time (CT) ^{1}H–^{13}C HMQC correlation map of the same sample recorded in H_2O and features the correlations of $Ile^{\delta 1}$ and Val^{γ}/Leu^{δ} methyl groups (114 observable methyl correlations including 2 from Leu in the 'LE' linker between the C-termini of the dimer and the six-residue His-tag). The quality of both amide and methyl correlation maps allows for a detailed NMR study of the dimer even at only moderately high spectrometer fields (600 MHz). *Bst*-YRS forms an exceptionally stable dimer: the dimer dissociation constant K_D of ~85 pM measured for the full-length *Bst*-YRS (Park and Bedouelle 1998). The interface between the two subunits of the dimer is comprised entirely of the residues in the N-terminal part of the protein (Fig. 1a), and a similar dissociation constant is therefore expected for the truncated variant of the enzyme. At room temperature, the molecular weight of ΔYRS corresponds to dimeric species based on size-exclusion chromatography elution time and PAGE electrophoresis under native conditions (Godoy-Ruiz, et al. 2011). At higher temperatures (up to 50 °C), ^{15}N T_1 and $T_{1\rho}$ relaxation times of ΔYRS measured on the [U-^{2}H; ^{15}N]-labeled sample, agree with those predicted for dimeric species (average ^{1}H-decoupled ^{15}N T_1 and $T_{1\rho}$ times of 2.4 s and 19 ms measured in ΔYRS at 40 °C, 600 MHz, corresponding to the isotropic correlation time of global molecular tumbling of ~35 ns).

At initial stages of the sequential assignment process when the first stretches of spin-system connectivities are mapped onto the amino-acid sequence of a protein, it is useful to identify as many 'starting points' corresponding to residues of unambiguous type as possible. The approach that selects amide correlations of alanines as 'starting points' has been adopted earlier for assignments of MSG (Tugarinov et al. 2002), using a modified 2D TROSY-HN(CACB) scheme (Salzmann et al. 1999; Tugarinov et al. 2002; Yang and Kay 1999) that is reproduced in Fig. 2a. When the magnetization resides on $^{13}C^{\beta}$, the terms $^{13}C_z^{\alpha}{}^{13}C_x^{\beta}$ are refocused by the ^{13}C RE-BURP pulse (Geen and Freeman 1991) with the phase $\phi 3$ (labeled with an asterisk in Fig. 2a) selective for the unique and narrow range of Ala $^{13}C^{\beta}$ chemical shifts, while all the other terms are eliminated by phase-cycling of the pulse and the two flanking gradients. The 2D TROSY-HN(CACB) correlation map of *Bst*-ΔYRS is shown in Fig. 2b and features the ^{1}H–^{15}N correlations of Ala (italicized) and a number of ^{1}H-^{15}N correlations of residues following alanines. To distinguish between these two types of correlations, the transfer through carbonyl nuclei can be used to provide correlations of amides following Ala exclusively (Ala + 1). Such a 2D HN(COCACB) map is shown in the inset of Fig. 2b.

Unique $^{13}C^{\beta}$ chemical shifts of Ser and Thr allow for the straightforward extension of this approach via selection of amides of Ser/Thr as starting points for assignments. Specifically, the adjustment of (1) the delay ζ in the scheme of Fig. 2a to $1/(4^{1}J_{C\alpha C\beta}) = 7$ ms, and (2) the length and resonance frequency of the $^{13}C\phi_3$ pulse selective for $^{13}C^{\alpha}$ and $^{13}C^{\beta}$ chemical shifts of Ser/Thr, retains the magnetization terms $^{13}C_z^{\alpha}{}^{13}C_x^{\beta}$ of Ser and Thr, while the same terms of other residue types are de-phased. Figure 2c shows the amide correlations of Ser and Thr in ΔYRS (italicized) and a number of correlations belonging to the amides of residues following Ser/Thr. Similarly, the 2D TROSY-HN(CO-CACB) map in the inset of Fig. 2c features only the amide correlations of residues following Ser/Thr (Ser/Thr + 1; prolines excluded). We note that the described simplification of the 2D ^{1}H–^{15}N TROSY correlation maps represents primarily a matter of 'convenience' for data interpretation, as correlations belonging to either Ala or Ser/Thr can be identified by inspection of the generally more sensitive 3D data sets. In some cases, however, the correlations of Thr $^{13}C^{\beta}$ (aliased in the ^{13}C dimensions of 3D HNCACB and HN(CO)CACB spectra) and Ser $^{13}C^{\beta}$ may (partially) overlap with the peaks of opposite phase in the 3D datasets leading to problems with their identification. In the two such cases encountered in ΔYRS, the Ser/Thr-selective HN(CACB) maps proved helpful for residue-type identification.

Although ~96 % of all expected intra-residual and ~95 % of inter-residual $^{13}C^{\alpha}$ and $^{13}C^{\beta}$ correlations could be observed in 3D TROSY-HNCACB and TROSY-HNCO-CACB data sets (Salzmann et al. 1999, Yang and Kay 1999) of ΔYRS at 600 MHz, many of the correlations are weak, and complete assignment of the backbone resonances from this pair of experiments only proves problematic. The main difficulty in establishing unambiguous connectivities from these two 3D data sets lies in the high level of degeneracy of ($^{13}C^{\alpha}$; $^{13}C^{\beta}$) pairs of chemical shifts among the residues of the same type adopting similar conformations (i.e. found in the same secondary structure elements). More sensitive 3D TROSY-HNCOCA and TROSY-HNCA data sets prove to be helpful for establishing correct connectivities in ΔYRS. As it was noted previously in the case of MSG (Tugarinov et al. 2002), 3D ^{15}N-separated NOE-TROSY experiment is very helpful in establishing connectivities between the amide correlations in α-helices and tight turns. About 85 % of all expected (strong) sequential HN-HN NOE contacts could be observed in the α-helical stretches of predominantly (76 %) helical ΔYRS.

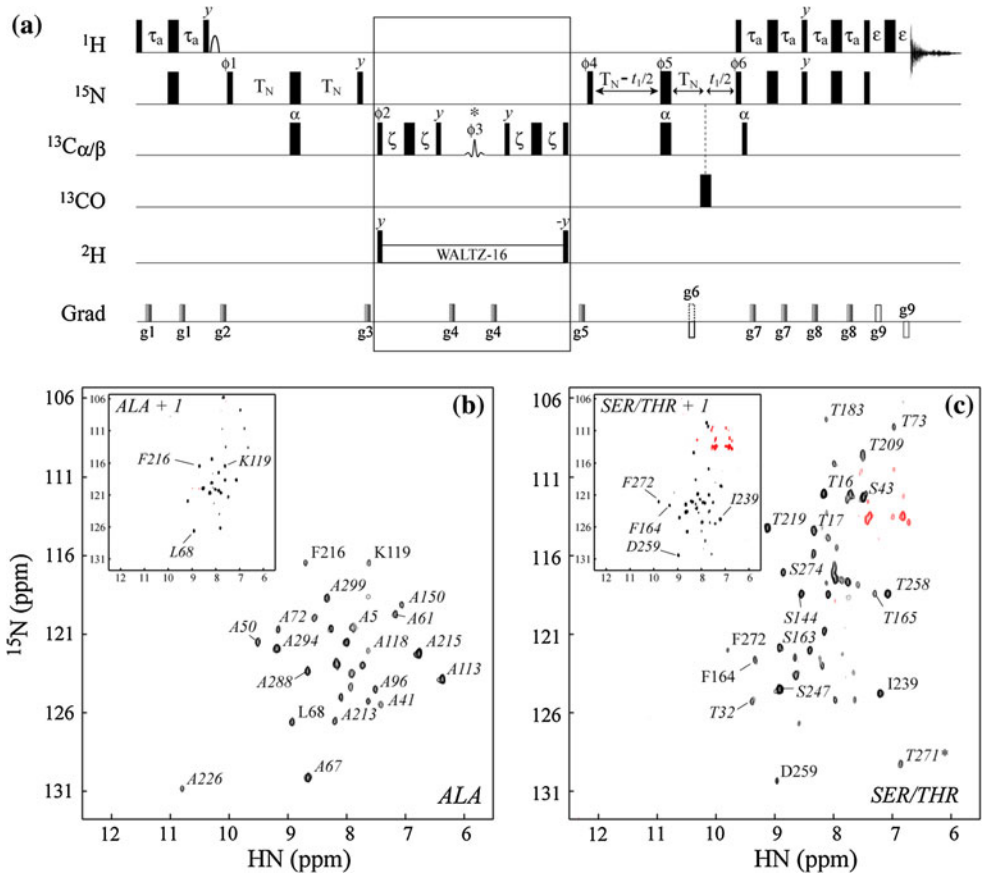

Fig. 2 **a** A modified 2D TROSY-HN(CACB) pulse scheme used for selective detection of Ala or Ser/Thr amide correlations. The details of experimental set-up can be found in Yang and Kay (1999) and Tugarinov et al. (2002). All narrow (wide) rectangular pulses are applied with the flip angles of 90°(180°) along the *x*-axis unless indicated otherwise. The ^{1}H(^{2}H; ^{15}N; $^{13}C^{\alpha/\beta}$; ^{13}CO) carriers are positioned at 4.7 (4.0; 119; 42; 176) ppm. All ^{1}H, ^{15}N and ^{13}C pulses are applied with maximum possible power unless indicated otherwise, while ^{2}H WALTZ-16 decoupling uses a 0.9 kHz field. The ^{1}H pulse shown with an arc is a 1.5-ms 90° water-selective pulse of rectangular shape applied on-resonance. The 90°(180°) ^{13}C pulses labeled with 'α' are applied at 57 ppm by phase modulation of the carrier (Boyd and Soffe 1989; Patt 1992) using a field strength of $\Delta/\sqrt{15}(\Delta/\sqrt{3})$ where Δ is the difference (in Hz) between $^{13}C^{\alpha}$ and ^{13}CO chemical shifts (Kay et al. 1990); likewise, the 180° ^{13}CO pulse is centered at 176 ppm by phase modulation of the carrier and is applied with a field strength of $\Delta/\sqrt{15}$. The ^{13}C shaped pulse with phase $\phi 3$ is a 3.3-ms RE-BURP pulse (Geen and Freeman 1991) (600 MHz) centered at 18.5 ppm by phase modulation of the carrier for selection of Ala $^{13}C^{\beta}$ (Tugarinov et al. 2002), and a 1.3-ms RE-BURP pulse centered at 65 ppm for selection of Ser/Thr $^{13}C^{\alpha}$ and $^{13}C^{\beta}$ (refocusing/inversion bandwidth of ±9.5 ppm at 600 MHz). Delays are: $\tau_a = 2.3$ ms; $T_N = 12.5$ ms; $\zeta = 5.0$ ms for Ala selection, and $\zeta = 7.0$ ms for Ser/Thr selection; $\varepsilon = 350$ μs. Only the delay ζ and the length/offset of the $^{13}C\phi_3$ RE-BURP pulse have to be changed in the element of the scheme enclosed in *rectangular box* to choose between Ala and Ser/Thr selection. The phase-cycle is: $\phi 1 = x,-x$; $\phi 2 = 2(x), 2(-x)$; $\phi 3 = 4(x), 4(y), 4(-x), 4(-y)$; $\phi 4 = y$; $\phi 5 = 8(x), 8(-x)$; $\phi 6 = x$; rec. $= 2(x,-x,-x,x, \ -x,x,x,-x)$. Quadrature detection in t_1 is achieved via the Rance-Kay scheme: for each t_1 value a pair of spectra is recorded with ($\phi 6 = x$; g6) and ($\phi 6 = -x$; −g6) and manipulated post-acquisition (Kay et al. 1992; Schleucher et al. 1993). The phase $\phi 4$ is inverted for each t_1 point (Marion et al. 1989). Durations and strengths of pulsed-field gradients in units of (ms; G/cm) are: g1 = (0.35; 5); g2 = (1.5; 20); g3 = (0.8; 12); g4 = (0.20; 20); g5 = (1.0; 10); g6 = (1.25; −30); g7 = (0.4; 5); g8 = (0.3; 8); g9 = (0.0625; 28.9). **b** 2D TROSY-HN(CACB) correlation map of *Bst*-ΔYRS (600 MHz; 40 °C) showing the amide correlations of Ala residues and a number of correlations belonging to the amides of residues following Ala. Selected Ala correlations are labeled with residue numbers in *italics*, while the correlations belonging to the amides of residues following Ala are shown in *plain font*. The *inset* shows the 2D TROSY-HN(COCACB) spectrum featuring only the amide correlations of residues following Ala (Ala + 1). **c** 2D TROSY-HN(CACB) correlation map of *Bst*-ΔYRS showing the amide correlations of Ser or Thr residues and some correlations belonging to the amides of residues following Ser/Thr. Selected Ser/Thr correlation are labeled with residue numbers in *italics*, while selected correlations belonging to the amides of residues following Ser/Thr are shown in *plain font*. The *inset* shows the 2D Ser/Thr-TROSY-HN(COCACB) spectrum with the amide correlations of residues following Ser/Thr only (Ser/Thr + 1). Net acquisition times of the 2D correlation maps varied from ∼12 h for Ala-HN(CACB) and Ala-HN(COCACB) data sets to ∼22 h for the data sets that select for Ser/Thr (Ser/Thr + 1)

Figure 3 illustrates how the connectivity between Val^{302} and Glu^{301} in one of the α-helices of ΔYRS is established from the triple-resonance experiments with the help of NOESY data. A region of the 2D ^{1}H–^{15}N TROSY map of ΔYRS with the amide correlations of Val^{302} and Glu^{301} is shown Fig. 3a, while b shows a region of the HN–HN plane of the 3D

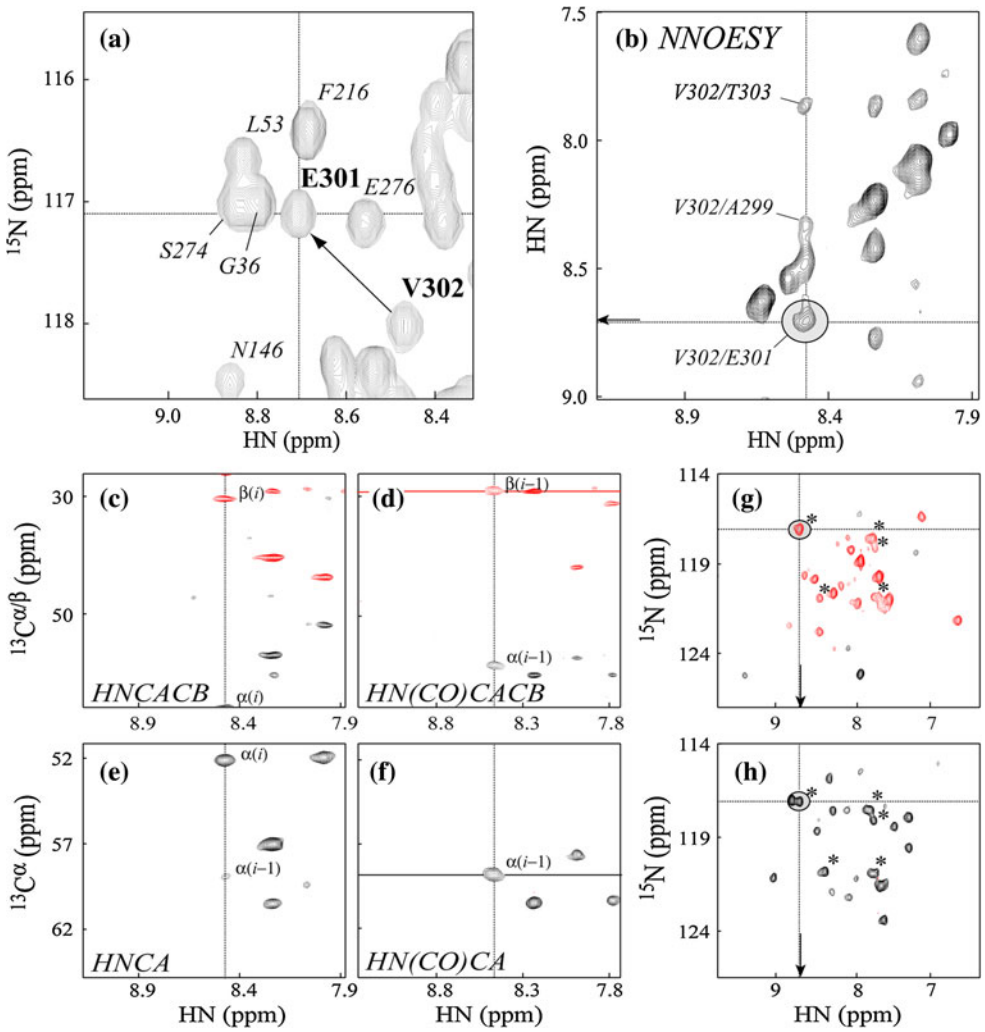

Fig. 3 **a** A region of the 2D ^{1}H-^{15}N TROSY map of *Bst*-ΔYRS highlighting the amide correlations of Val^{302} and Glu^{301}. **b** A region of the HN-HN plane of the 3D ^{15}N-separated NOE-TROSY data set drawn at the ^{15}N chemical shift of Val^{302} (118.02 ppm). The NOE connectivity between the amides of Val^{302} and Glu^{301} is *circled* and *highlighted*. The cross-peaks between the amide proton of Val^{302} and the amide protons of residues i + 1 (Thr^{303}) and i − 3 (Ala^{299}) in the same α-helix are labeled. A region of the HN-^{13}C$^{\alpha/\beta}$ plane of the 3D TROSY-HNCACB (**c**) and TROSY-HNCOCACB (**d**) datasets plotted at the amide ^{15}N chemical shifts of Val^{302}. A region of the HN-^{13}C$^{\alpha}$ plane of the 3D TROSY-HNCA (**e**), and TROSY-HNCOCA (**f**) spectra plotted at the same ^{15}N chemical shift as in **c**–**d**. The *vertical dotted lines* in (**c**–**f**) are drawn at the HN chemical shift of Val^{302} (8.47 ppm) A region of the HN-^{15}N plane of the 3D TROSY-HNCACB (**g**) and TROSY-HNCA (**h**) data sets plotted at the ^{13}C chemical shifts of the previous residue, Glu^{301}, indicated by *horizontal red line* in **d** (^{13}C$^{\beta}$ = 28.8 ppm) and *horizontal black line* in f (^{13}C$^{\alpha}$ = 58.8 ppm). The cross-peaks appearing at the (HN, ^{15}N) chemical shifts of Glu^{301} is *circled* and *highlighted* in **g**–**h**. The peaks marked with *asterisks* have the same (HN, ^{15}N) chemical shifts in panels (**g**) and (**h**) and represent potential candidates for assignment of Glu^{301}. Negative peaks are shown with *red contours*. All the spectra have been processed with NMRPipe/NMRDraw software (Delaglio et al. 1995) and analyzed with the NMRView program (Johnson and Blevins 1994) and tcl/tk scripts written in-house

^{15}N-separated NOE-TROSY data set drawn at the ^{15}N chemical shift of Val^{302} (118.02 ppm). The regions of the HN-^{13}C planes of the 3D TROSY-HNCACB (Fig. 3c), TROSY-HNCOCACB (Fig. 3d), TROSY-HNCA (Fig. 3e), and TROSY-HNCOCA (Fig. 3f) datasets are all plotted at the same ^{15}N chemical shifts of Val^{302}. Of note, HNCACB and HNCOCACB spectra are optimized for detection of ^{13}C$^{\beta}$ correlations by setting the delay ζ in Fig. 2a to 5.5 ms—hence, typically, somewhat higher intensities of ^{13}C$^{\beta}$ peaks are observed (red contours in Fig. 3c, d). A region of the HN-^{15}N cross-sections of the 3D TROSY-HNCACB and TROSY-HNCA data sets is plotted in Fig. 3g and h, respectively, at the ^{13}C chemical shifts of the previous residue, Glu^{301}, indicated by the horizontal red line (^{13}C$^{\beta}$ = 28.8 ppm) and the horizontal black line (^{13}C$^{\alpha}$ = 58.8 ppm) in panels (3d) and (f). The peaks marked with asterisks in Fig. 3g and h have the same (HN, ^{15}N) chemical shifts and represent potential candidates for assignment of the amide of the previous residue, Glu^{301}.

However, the NOE cross-peak between the amides of Val^{302} and Glu^{301} (circled and highlighted in Fig. 3b) helps to choose among these possibilities the right assignment for the amide of Glu^{301} according to the observed HN shift of the Val^{302}/Glu^{301} cross-peak: 8.71 ppm in the (vertical) HN dimension of Fig. 3b, and the (horizontal) HN dimension of Fig. 3g and h, as indicated with arrows in panels (b) and (g–h). Note that the cross-peaks between the amide proton of Val^{302} and the amide protons of residues i + 1 (Thr^{303}) and i − 3 (Ala^{299}) in the same α-helix of ΔYRS can also be easily identified in the same plane of the NOE-TROSY spectrum (Fig. 3b).

Identification of residue types poses another difficulty in the assignment process. The advantage of performing practically simultaneous backbone and $Ile^{\delta 1}$, Leu^{δ}, Val^{γ} (ILV)-methyl assignments stems from the possibility of confirming the types of residues in every instance when Ile, Val or Leu is encountered in the protein sequence. Although the transfer of magnetization from ILV methyls to backbone amides would allow recording of the simplified 2D ^{1}H-^{15}N correlation maps selective for these residue types (similar to Ala/Ser/Thr selection in Fig. 2) we have chosen to use methyl-detected 'out-and-back' 3D HMCM(CG)CBCA experiment (Tugarinov and Kay 2003) for determination of the chemical shifts of $^{13}C^{\alpha}$ and $^{13}C^{\beta}$ nuclei of ILV residues and concomitant confirmation of their residue types. ILV residues comprise 21 % of the ΔYRS amino-acid content, and the juxtaposition of ^{13}C ($^{13}C^{\alpha}$,$^{13}C^{\beta}$) correlations obtained in HNCACB and HMCM(CG)CBCA data sets helped to identify/confirm the types of a total of 58 residues in ΔYRS. Figures 4a and c shows the strips from the 3D TROSY-HNCOCACB (left panels) and TROSY-HNCACB (right panels) plotted at the amide (^{1}H; ^{15}N) chemical shifts of Ile^{239} (4a) and Val^{13} (4c), while the strips from the 3D HMCM(CG)CBCA data set drawn at the (^{1}H; ^{13}C) chemical shifts of Ile^{239} $\delta 1$ methyl, and two Val^{13} γ methyls are plotted in Fig. 4b and d, respectively. Because both HNCACB and HMCM(CG)CBCA data sets are recorded in H_2O using the same [U-^{2}H,^{15}N,^{13}C; Ileδ1-{$^{13}CH_3$}; Leu, Val-{$^{13}CH_3$/$^{12}CD_3$}]-labeled sample, the chemical shifts of $^{13}C^{\alpha}$ and $^{13}C^{\beta}$ nuclei are exactly the same in the two data sets, with deuterium isotope shifts affecting both spectra in identical manner. Note that the ($^{13}C^{\alpha}$; $^{13}C^{\beta}$) chemical shifts of Ile^{239} are somewhat unusual for isoleucine (57.5; 33.5 ppm) and can be (mis)attributed to a number of other residue types. Likewise, ($^{13}C^{\alpha}$; $^{13}C^{\beta}$) chemical shifts of Val^{13} (60.7; 31.7 ppm) do not allow unambiguous identification of the type of this residue without recourse to the HMCM(CG)CBCA data set. Of note, the protonation of ILV methyls in the sample of ΔYRS amounts to addition of only 8 % more protons to the protein, and by all measures is not significantly detrimental to the quality of ^{1}H-^{15}N-TROSY spectra. Practically complete (96 %) assignments of ^{1}HN, ^{15}N $^{13}C^{\alpha}$, $^{13}C^{\beta}$ and ^{13}CO chemical shifts, complete (100 %) assignments of (^{1}H, ^{13}C) shifts of $Ile^{\delta 1}$ and Val^{γ} methyls, and assignments of 90 % of Leu^{δ} methyl groups have been achieved in *Bst*-ΔYRS. The remaining Leu^{δ} correlations are weak in constant-time (CT)-HMQC maps possibly indicating conformational exchange. Methyl-detected Val-HMCM(CBCA)CO and Ile/Leu-HMCM(CGCBCA)CO experiments (Tugarinov and Kay 2003) have confirmed the assignments of Valγ and Ileδ1 methyls of ΔYRS, and were necessary to resolve ambiguities in assignments of 12 Leu methyls arising from (near) degeneracy of ($^{13}C^{\alpha}$; $^{13}C^{\beta}$) pairs of chemical shifts.

Figure 5 shows the deviations of $^{13}C^{\alpha}$, $^{13}C^{\beta}$ and ^{13}CO chemical shifts of ΔYRS from the random coil values. The patterns of these deviations as well as the NMR-predicted secondary structure indicators obtained from chemical shift

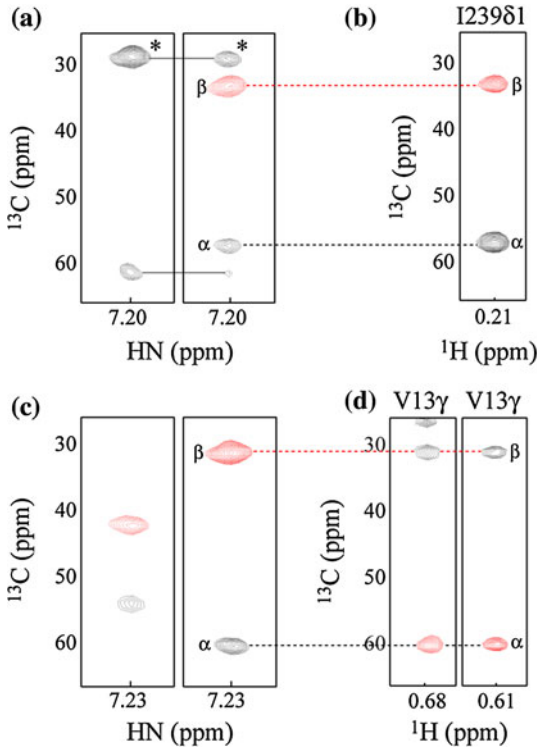

Fig. 4 Selected strips drawn from the 3D TROSY-HNCOCACB, 3D TROSY-HNCACB, and HMCM(CG)CBCA data sets recorded on [U-^{2}H,^{15}N,^{13}C; Ileδ1-{$^{13}CH_3$}; Leu,Val-{$^{13}CH_3$/$^{12}CD_3$}]-*Bst*-ΔYRS: *Strips* from the 3D TROSY-HNCOCACB (*left panel*) and TROSY-HNCACB (*right panel*) plotted at the amide (^{1}H; ^{15}N) chemical shifts of **a** Ile^{239}: (7.19; 124.7) ppm, and **c** Val^{13}: (7.23; 115.1) ppm; Strips from the 3D HMCM(CG)CBCA data set drawn at the (^{1}H; ^{13}C) chemical shifts of (**b**) Ile^{239} $\delta 1$ methyl: (0.21; 8.9) ppm, and (**c**) two Val^{13} γ methyls: (0.61; 21.2) ppm and (0.68; 21.7) ppm. The correlations to $^{13}C^{\beta}$ of Thr^{238} are aliased in the ^{13}C dimension and marked with *asterisks* in (**a**). *Red dashed lines* connect $^{13}C^{\beta}$ correlations, while *black dashed lines* connect $^{13}C^{\alpha}$ correlations between the HNCACB (**a**, **c**) and HMCM(CG)CBCA (**b**, **d**) data sets. Relative phases of $^{13}C^{\alpha}$ and $^{13}C^{\beta}$ correlations in HMC(CG)CBCA spectra unambiguously distinguish between Ile and Val side-chains

index (CSI) consensus analysis of $^{13}C^{\alpha}$, $^{13}C^{\beta}$ and ^{13}CO chemical shifts (Spera and Bax 1991; Williamson 1990; Wishart and Case 2002; Wishart and Sykes 1994a, b; Wishart et al. 1992) are in excellent agreement with those expected from the crystal structure of ΔYRS (Brick and Blow 1987). Since carbonyl chemical shifts have not been evolved in any of the spectra used for assignments, ^{13}CO chemical shifts have been assigned separately from 3D TROSY-HNCO spectra. Interestingly, despite that the carbonyl chemical shifts are typically affected by hydrogen bonding effects, the deviations of ($^{13}C^{\alpha}$; ^{13}CO) pairs of chemical shifts generally serve as more reliable predictors of secondary structure than the ($^{13}C^{\alpha}$; $^{13}C^{\beta}$) pairs. With only three exceptions—Trp[9], Arg[10] and Thr[134]—the non-proline residues of ΔYRS whose amide correlations could not be identified (enclosed in rectangular boxes in Fig. 5) belong to non-hydrogen-bonded amides located in the loops or occupying one of the first three positions of different α-helices in the ΔYRS structure. Among notably anomalous backbone amide ^{1}HN and ^{15}N chemical shifts in ΔYRS are those of Val[31]: 12.0 and 134.4 ppm, respectively. The inspection of the YRS crystal structure shows that the amide group of Val[31] forms a (strong) hydrogen bond with the $N^{\delta 1}$ position in the imidazole ring of His[63] ($NH\cdots N^{\delta 1}$ distance of 1.9 Å) explaining the unusual downfield shifts of both ^{1}HN and ^{15}N nuclei (Wagner, et al. 1983). Unusually large positive deviations from random coil $^{13}C^{\alpha}$ chemical shifts ($\Delta^{13}C^{\alpha} > 7$ ppm) are noted for two threonines in ΔYRS—Thr[54] with ($^{13}C^{\alpha}$; $^{13}C^{\beta}$) chemical shifts of (68.9; 66.4) ppm and Thr[303] with ($^{13}C^{\alpha}$; $^{13}C^{\beta}$) shifts of (68.9; 66.8) ppm, both located in α-helices (Fig. 5)—leading to 'swapping' of the relative ($^{13}C^{\alpha}$; $^{13}C^{\beta}$) chemical shift positions in these two residues.

In summary, we report that practically complete assignments of ^{1}HN, ^{15}N, $^{13}C^{\alpha}$, $^{13}C^{\beta}$, ^{13}CO and ILV methyl (^{1}H, ^{13}C) chemical shifts of the truncated form of *Bst*-Tyrosyl tRNA Synthetase, a 319-residue homodimer, are feasible using a single [U-^{2}H,^{15}N,^{13}C; Ileδ1-{$^{13}CH_3$};

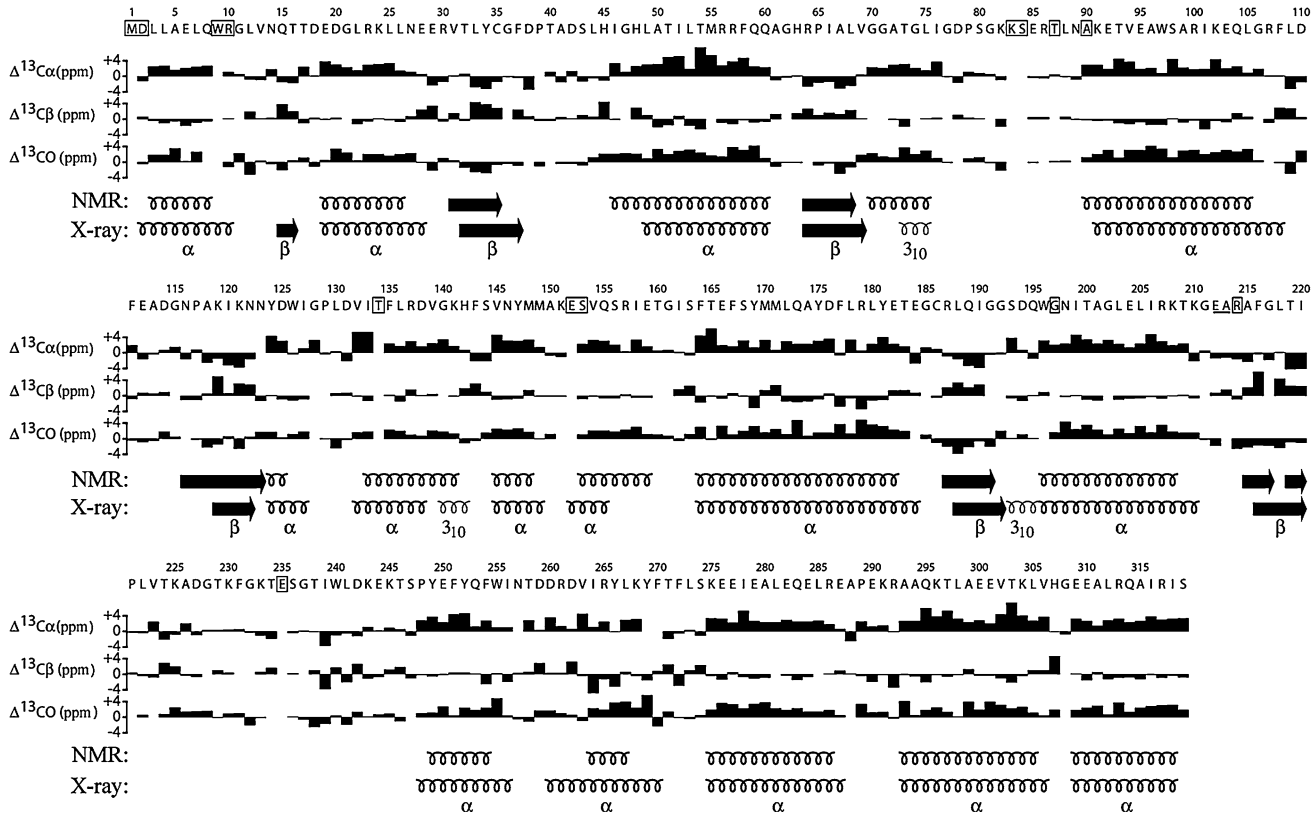

Fig. 5 Deviations of $^{13}C^{\alpha}$, $^{13}C^{\beta}$ and ^{13}CO chemical shifts of ΔYRS from the random coil values. The indicated secondary structure elements are based on the chemical shift index (CSI) consensus analysis of $^{13}C^{\alpha}$, $^{13}C^{\beta}$ and ^{13}CO chemical shifts (Wishart and Sykes 1994a) (*top rows*) and the X-ray structure, PDB id 1tyd (Brick and Blow 1987), *bottom rows*. Random coil chemical shifts have been taken from the reduced database of protein chemical shifts in the BioMagResBank, BMRB (http://www.bmrb.wisc.edu) and corrected for isotope effects (Gardner et al. 1997, Venters, et al. 1996). Non-proline residues of ΔYRS whose amide (^{1}H–^{15}N) correlations have not been identified in the spectra are enclosed in *rectangular boxes*. The two residues *underlined* with a *solid line* (Glu[212] and Ala[213]) are missing from the X-ray structure. Note that the PDB entry 1tyd has serine at position 51 (Ser[51]) instead of Thr, which is not consistent with either the genomic sequence of *Bst*-YRS or the PDB entries of full-length *Bst*-YRS (PDB id's 1TS1, 2TS1 and 3TS1 (Brick et al. 1989))

Leu,Val-{$^{13}CH_3/^{12}CD_3$}]-labeled protein sample. Protonation of ILV residues at methyl positions does not appreciably detract from the quality of TROSY triple resonance data. The assignments are assisted by: (1) selection of ^{1}H-^{15}N correlations of certain residue types (Ala, Thr/Ser) that simplifies 2D ^{1}H–^{15}N TROSY maps and facilitates identification of 'starting points' for assignments, (2) identification of ILV residue types using methyl-detected 'out-and-back' HMCM(CG)CBCA experiment that (in the absence of deuterium isotope shifts) provides $^{13}C^{\alpha}$, $^{13}C^{\beta}$ correlations of ILV residues with exactly the same chemical shifts as the intra-residual correlations in HNCACB data sets, and (3) by 3D TROSY-NOE data that typically show strong sequential HN-HN NOE connectivities in the helical segments of the protein. In consistency with our previous study (Godoy-Ruiz et al. 2011), no indications of structural asymmetry (differences in the chemical shifts of the two subunits of the homodimer) have been observed in either amide- or methyl-detected NMR experiments. The apparent structural symmetry of the homodimeric YRS in the absence of ligands contradicts earlier findings from extensive biochemical and kinetic experiments (Ward and Fersht 1988a), and poses a dilemma that can potentially be resolved via application of solution NMR techniques to heterodimeric YRS/ΔYRS constructs—for example, an investigation of how YRS/ΔYRS with different isotope labeling of the two subunits responds to binding of ligands on a pre-determined subunit. Although chemical shifts are very sensitive to the local environment, the measurement of backbone ^{1}H–^{15}N residual dipolar couplings may offer further evidence regarding the symmetry of ΔYRS. It is noteworthy that the asymmetry of ΔYRS might have a 'dynamic' character in the sense that the inter-conversion between catalytically competent/incompetent (C/C′) and incompetent/competent (C′/C) conformations of the dimer might occur fast on the chemical shift time-scale resulting in a single set of peaks in NMR spectra. The assignments of ΔYRS reported here will pave the way for further investigations that are bound to confirm or disprove this hypothesis.

Acknowledgments The authors thank Prof. Paul Paukstelis (University of Maryland) for the gift of the plasmid encoding full-length *Bst*-YRS from which the plasmid for ΔYRS expression was derived, and Prof. Eric First (Louisiana State University Health Center) for stimulating discussions. Backbone and ILV methyl assignments of *Bst*-ΔYRS have been deposited to BMRB data bank, http://www.bmrb.wisc.edu, entry #18588.

References

Boyd J, Soffe N (1989) Selective excitation by pulse shaping combined with phase modulation. J Magn Reson 85:406–413

Brick P, Blow DM (1987) Crystal structure of a deletion mutant of a tyrosyl-tRNA synthetase complexed with tyrosine. J Mol Biol 194:287–297

Brick P, Bhat TN, Blow DM (1989) Structure of tyrosyl-tRNA synthetase refined at 2.3A resolution. Interaction of the enzyme with the tyrosyl adenylate intermediate. J Mol Biol 208:83–98

Delaglio F, Grzesiek S, Vuister GW, Zhu G, Pfeifer J, Bax A (1995) NMRPipe: a multidimensional spectral processing system based on UNIX pipes. J Biomol NMR 6:277–293

Fersht AR (1975) Demonstration of two active sites on a monomeric aminoacyl-tRNA synthetase. Possible roles of negative cooperativity and half-of-the-sites reactivity in oligomeric enzymes. Biochemistry 14:5–12

Fersht AR (1987) Dissection of the structure and activity of the tyrosyl-tRNA synthetase by site-directed mutagenesis. Biochemistry 26:8031–8037

Fersht A (2002) Structure and mechanism in protein science. Freeman & Co., New York

Gardner KH, Rosen MK, Kay LE (1997) Global folds of highly deuterated, methyl protonated proteins by multidimensional NMR. Biochemistry 36:1389–1401

Geen H, Freeman R (1991) Band-selective radiofrequency pulses. J Magn Reson 93:93–141

Godoy-Ruiz R, Krejcirikova A, Gallagher DT, Tugarinov V (2011) Solution NMR evidence for symmetry in functionally or crystallographically asymmetric homodimers. J Am Chem Soc 133:19578–19581

Guijarro JI, Pintar A, Prochnicka-Chalufour A, Guez V, Gilquin B, Bedouelle H, Delepierre M (2002) Structure and dynamics of the anticodon arm binding domain of *Bacillus stearothermophilus* Tyrosyl-tRNA synthetase. Structure 10:311–317

Johnson BA, Blevins RA (1994) NMRView: a computer program for the visualization and analysis of NMR data. J Biomol NMR 4:603–614

Kay LE, Ikura M, Tschudin R, Bax A (1990) Three-dimensional triple-resonance NMR spectroscopy of isotopically enriched proteins. J Magn Reson 89:496–514

Kay LE, Keifer P, Saarinen T (1992) Pure absorption gradient enhanced heteronuclear single quantum correlation spectroscopy with improved sensitivity. J Am Chem Soc 114:10663–10665

Marion D, Ikura M, Tschudin R, Bax A (1989) Rapid recording of 2D NMR spectra without phase cycling. Application to the study of hydrogen exchange in proteins. J Magn Reson 85:393–399

Park YC, Bedouelle H (1998) Dimeric tyrosyl-tRNA synthetase from *Bacillus stearothermophilus* unfolds through a monomeric intermediate. A quantitative analysis under equilibrium conditions. J Biol Chem 273:18052–18059

Patt SL (1992) Single- and multiple-frequency-shifted laminar pulses. J Magn Reson 96:94–102

Salzmann M, Wider G, Pervushin K, Senn H, Wüthrich K (1999) TROSY-type triple resonance experiments for sequential NMR assignment of large proteins. J Am Chem Soc 121:844–848

Schleucher J, Sattler M, Griesinger C (1993) Coherence selection by gradients without signal attenuation: application to the three-dimensional HNCO experiment. Angew Chem Int Ed Engl 32:1489–1491

Spera S, Bax A (1991) Empirical correlation between protein backbone conformation and C^{α} and C^{β} ^{13}C nuclear magnetic resonance chemical shifts. J Am Chem Soc 113:5490–5492

Tugarinov V, Kay LE (2003) Ile, Leu, and Val methyl assignments of the 723-residue malate synthase G using a new labeling strategy and novel NMR methods. J Am Chem Soc 125:13868–13878

Tugarinov V, Muhandiram R, Ayed A, Kay LE (2002) Four-dimensional NMR spectroscopy of a 723-residue protein: chemical shift assignments and secondary structure of malate synthase G. J Am Chem Soc 124:10025–10035

Venters RA, Farmer BT, Fierke CA, Spicer LD (1996) Characterizing the use of perdeuteration in NMR Studies of large proteins: ^{13}C, ^{15}N and ^{1}H assignments of human carbonic anhydrase II. J Mol Biol 264:1101–1116

Wagner G, Pardi A, Wüthrich K (1983) Hydrogen bond length and proton NMR chemical shifts in proteins. J Am Chem Soc 105: 5948–5957

Ward WH, Fersht AR (1988a) Asymmetry of tyrosyl-tRNA synthetase in solution. Biochemistry 27:1041–1049

Ward WH, Fersht AR (1988b) Tyrosyl-tRNA synthetase acts as an asymmetric dimer in charging tRNA. A rationale for half-of-the-sites activity. Biochemistry 27:5525–5530

Waye MM, Winter G, Wilkinson AJ, Fersht AR (1983) Deletion mutagenesis using an 'M13 splint': the N-terminal structural domain of tyrosyl-tRNA synthetase (*B. stearothermophilus*) catalyses the formation of tyrosyl adenylate. EMBO J 2:1827–1829

Williamson MP (1990) Secondary-structure dependent chemical shifts in proteins. Biopolymers 29:1423–1431

Wishart DS, Case DA (2002) Use of chemical shifts in macromolecular structure determination. Methods Enzymol 338:3–34

Wishart DS, Sykes BD (1994a) The ^{13}C chemical-shift index: a simple method for identification of protein secondary structure using ^{13}C chemical shift data. J Biomol NMR 4:171–180

Wishart DS, Sykes BD (1994b) Chemical shifts as a tool for structure determination. Methods Enzymol 239:363

Wishart DS, Sykes BD, Richards FM (1992) The chemical shift index: a fast and simple method for the assignment of protein secondary structure through NMR spectroscopy. Biochemistry 31:1647–1651

Yang D, Kay LE (1999) TROSY triple resonance four-dimensional NMR spectroscopy of a 46 ns tumbling protein. J Am Chem Soc 121:2571–2575